Knockout of Nuclear High Molecular Weight FGF2 Isoforms in Mice Modulates Bone and Phosphate Homeostasis*

Collin Homer-Bouthiette[‡], Thomas Doetschman[§], Liping Xiao[‡1], and Marja M. Hurley[‡2]

From the [‡]Department of Medicine, Institute for Systems Genomics, University of Connecticut Health Center, Farmington, Connecticut 06030 and the [§]B105 Institute and Department Cellular and Molecular Medicine, University of Arizona, Tucson, Arizona 85724-5217

Background: FGF2 isoforms have differential effects on bone and phosphate homeostasis.
Results: Knock-out of HMWFGF2 increased bone density and reduced bone *Fgf23*, *Sost* mRNA, and serum sclerostin.
Conclusion: HMWKO mice display increased bone mineralization and normal serum phosphate due to modulation of bone-related genes.
Significance: Modulation of HMWFGF2 could possibly be utilized in development of therapeutic targets to treat osteomalacia and phosphate disorders.

We previously reported that targeted overexpression of the fibroblast growth factor 2 (FGF2) high molecular weight (HMW) isoforms in osteoblastic lineage cells in mice resulted in phenotypic changes, including dwarfism, rickets, osteomalacia, hypophosphatemia, increased serum parathyroid hormone, and increased levels of the phosphatonin FGF23 in serum and bone. This study examined the effects of genetically knocking out the FGF2HMW isoforms (HMWKO) on bone and phosphate homeostasis. HMWKO mice were not dwarfed and had significantly increased bone mineral density and bone mineral content in femurs and lumbar vertebrae when compared with the wild-type (WT) littermates. Micro-computed tomography analysis of femurs revealed increased trabecular bone volume, thickness, number, and connective tissue density with decreased trabecular spacing compared with WT. In addition, there was significantly decreased cortical porosity and increased cortical thickness and sub-periosteal area in femurs of HMWKO. Histomorphometric analysis demonstrated increased osteoblast activity and diminished osteoclast activity in the HMWKO. *In vitro* bone marrow stromal cell cultures showed there was a significant increase in alkaline phosphatase-positive colony number at 1 week in HMWKO. At 3 weeks of culture, the mineralized area was also significantly increased. There was increased expression of osteoblast differentiation marker genes and reduced expression of genes associated with impaired mineralization, including a significant reduction in *Fgf23* and *Sost* mRNA. Normal serum phosphate and parathyroid hormone were observed in HMWKO mice. This study demonstrates a significant negative impact of HMWFGF2 on biological functions in bone and phosphate homeostasis in mice.

Fibroblast growth factor 2 (FGF2), which is expressed in osteoblasts and stromal cells and then stored in the surrounding extracellular matrix (1), has a significant impact on bone formation through modulation of distinct signaling pathways that regulate osteoblast differentiation, matrix mineralization, and phosphate (P_i) homeostasis in mice. In humans, there are several FGF2 protein isoforms as follows: high molecular weight (HMW)[3] isoforms (22, 22.5, and 24 kDa) and a low molecular weight (LMW/18 kDa) isoform (2). The LMW isoform is initiated from a traditional AUG start codon, whereas the HMW isoforms are translated from individual nonconventional CUG codons upstream of the LMW start site (3). In rodents, there are three isoforms as follows: two HMW isoforms (20.5 and 21 kDa) as well as a LMW isoform (17.5 kDa) (4). The HMW and LMW isoforms have differing biological functions in regulating bone homeostasis. The LMW isoform is transported out of the cell and functions as an autocrine/paracrine growth factor (5). When all of the FGF2 isoforms are overexpressed in mice, the mice displayed a dwarf phenotype (6) and had decreased bone mass and bone mineral density (BMD) (7). Interestingly, transgenic mice overexpressing only the LMW isoform in osteoblastic lineage cells had a significantly increased BMD and bone mass with normal serum phosphate (8). HMW isoforms have a nuclear localization sequence and remain in the nucleus to function as an intracrine factor (9). In contrast to LMWTg mice, HMWTg mice, overexpressing the HMW FGF2 isoforms in osteoblastic lineage, were significantly hypophosphatemic and had significantly decreased BMD and bone mass (10). Mechanistically, these differences were shown to be due, in part, to modulation of the Fgf23/Klotho signaling pathway (10). *In vitro* bone formation studies using bone marrow stromal cells (BMSCs) from HMWTg mice demonstrated a significant decrease in pro-osteoblast differentiation and mineralization gene expressions such as osterix, osteocalcin, and

---

[1] To whom correspondence may be addressed: Dept. of Medicine, University of Connecticut Health Center, 263 Farmington Ave., Farmington, CT 06030. Tel.: 860-679-2830; Fax: 860-679-1875; E-mail: xiao@uchc.edu.
[2] To whom correspondence may be addressed: Dept. of Medicine, University of Connecticut Health Center, 263 Farmington Ave., Farmington, CT 06030. Tel.: 860-679-2830; Fax: 860-679-1875; E-mail: hurley@nso1.uchc.edu.

[3] The abbreviations used are: HMW, high molecular weight; PTH, parathyroid hormone; LMW, low molecular weight; Tg, transgenic; BMSC, bone marrow stromal cell; BV, bone volume; TV, total volume; MAR, mineral apposition rate; BS, bone surface; BFR, bone formation rate; MS, mineralizing surface; micro-CT, micro-computed tomography; BMD, bone mineral density; BMC, bone mineral content.

dentin matrix acidic phosphoprotein 1 (*DMP1*) as well as a significant increase in inhibitory matrix Gla protein (*Mgp*) and *Fgf23* (11).

The phosphatonin, FGF23, plays an important role in bone and P_i homeostasis, is secreted by osteoblasts/osteocytes, and acts both locally (paracrine) and systemically (endocrine) (10, 12). As an endocrine hormone, FGF23 is released into the bloodstream, increases P_i wasting, and modulates vitamin D homeostasis via its effects on the kidneys (13). FGF23 signals in the kidney by interacting with Klotho (14), an anti-aging protein that is not found in bone, and FGF receptor(s) (15–17) to activate downstream signaling pathways, including the MAPK/ERK pathway (11). This in turn inhibits the expression of the sodium-phosphate transporter 2a (Npt2a) (18). The decrease in Npt2a results in reduced P_i reabsorption in the renal proximal tubules (19) resulting in both phosphaturia and hypophosphatemia. This results in less P_i being available for bone homeostasis and repair because phosphate is necessary to form hydroxyapatite, which is the mineral in bone (20). P_i balance is critical for proper bone formation. Overexpression of HMW FGF2, and consequently FGF23, lessens the body's ability to efficiently produce and repair bone tissue (10). FGF23, when overexpressed, has also been reported to negatively regulate bone formation independently of the Klotho pathway, which modulates P_i homeostasis (21). Therefore, the HMW FGF2 isoform may have a greater impact on bone homeostasis than on serum P_i levels.

The aims of our study were to characterize the phenotype of a murine model in which only the HMW isoforms of FGF2 were deleted and to more precisely determine the role of HMW FGF2 in bone formation and phosphate regulation. As stated previously and similar to humans, mice have both HMW and LMW isoforms of FGF2, although mice only have two HMW isoforms (21 and 22 kDa) (22). Of potential clinical relevance, we previously reported that the HMW isoforms were increased in bones of the Hyp mouse (10), a murine model of human X-linked hypophosphatemic rickets. Therefore, this study examined whether there were changes in the expression patterns of genes that are related to bone matrix abnormalities in human disorders such as X-linked hypophosphatemic rickets, as well as autosomal dominant and recessive hypophosphatemic rickets/osteomalacia, in the presence or absence of the HMW FGF2 isoforms. Mouse models of human phosphate wasting disorders include the Hyp mouse in which Phex gene is knocked out (X-linked hypophosphatemic rickets) (23), *Dmp1* KO (autosomal recessive hypophosphatemic rickets) (24), and FGF23Tg (autosomal dominant hypophosphatemic rickets) (25) that mimic the human skeletal conditions. *Phex*, *Dmp1*, and *Fgf23* all play important roles in the bone-renal axis (26). *Dmp1* is a SIBLING (short integrin-binding ligand-interacting glycoprotein) that has an ASARM (acidic serine aspartate-rich MEPE-associated) motif, which interacts with Phex to down-regulate expression of Fgf23 (27). The MEPE-ASARM protein has been shown to competitively bind Phex, inhibiting Dmp1 activation (26). We also examined whether *Mgp*, the calcification inhibitor (28), was altered in bones of HMWKO mice, since we previously observed significantly elevated levels in bones of HMWTg mice (10). The results of this novel study

show that mice in which the HMW isoforms are knocked out present with normal serum phosphate, significantly increased BMD and bone mineral content (BMC), as well as increased expression of bone mineralization factors and decreased expression of inhibitors of bone formation.

EXPERIMENTAL PROCEDURES

HMWFgf2KO Mice—The HMWKO mice were generated at the GEMM Core at the University of Arizona by gene-targeted introduction of polymorphisms to remove the alternative CUG codon start sites required to translate the HMW isoforms of FGF2 (29). Heterozygote HMWFgf2+/− mice that are maintained on a Black/Swiss/129 Sv background were bred and housed in the transgenic facility in the Center for Laboratory Animal Care at the University of Connecticut Health Center. Genotyping of mice was performed using a method described previously (29). The University of Connecticut Health Center, Institutional Animal Care and Use Committee, approved all animal procedures. Two-month-old male HMWKO mice and their WT littermates were used for this study. The mice were sacrificed utilizing the approved CO_2 method of euthanasia.

Biochemistry—Blood was collected from euthanized animals by cardiac puncture. After clotting, the blood was spun, and serum was collected. Serum phosphate and calcium were measured using the Phosphorus Liqui-UV (StanBio Laboratory, TX) and CALCIUM (CPC) REAGENT SET (Eagle Diagnostics, Cedar Hill, TX), respectively. Serum FGF23 was measured using a kit purchased from Immunotopics Inc. (Carlsbad, CA), and serum PTH was determined using a mouse intact PTH enzyme-linked immunosorbent assay kit (Immunotopics) according to the manufacturer's instructions.

Faxitron X-ray—X-ray pictures of the whole mouse were taken using a SYSTEM MX 20 from Faxitron X-ray Corp. (Wheeling, IL). X-ray images were taken under constant conditions (25 kV, 20-s exposure at 4.5 magnification).

Dual Beam X-ray Absorptiometry—Dual beam x-ray absorptiometry imaging was performed using the LunarPIXImus2 (GE Medical Systems) densitometer to measure bone mineral density and bone mineral content for both *in vivo* and excised bones.

Micro-Computed Tomography (Micro-CT) Scanning of Femurs—Analysis of the metaphyseal cancellous bones of the distal femurs was performed as described previously (30) with micro-CT instrumentation (μCT20, Scanco Medical AG, Bassersdorf, Switzerland). Using two-dimensional data from scanned slices, three-dimensional analysis was conducted to calculate morphometric parameters defining micro-architecture, including bone volume density, bone volume (BV)/total volume (TV), trabecular number, trabecular thickness, trabecular spacing, connective tissue density, degree of anisotropy, sub-periosteal area, cortical mask, cortical porosity, and cortical thickness.

Bone Histomorphometry—Mice were labeled with calcein 7 days and xylenol orange 2 days prior to sacrifice, respectively. Femurs were isolated and fixed in 10% formalin. Bones were then placed overnight in 30% sucrose dissolved in PBS and embedded in Cryomatrix. The Cryomatrix block containing each undecalcified femur was oriented in the block holder to

TABLE 1
Primers used in qRT-PCR

β-Actin	5′–ATGGCTGGGGTGTTGAAGGT–3′	5′–ATCTGGCACCACACCTTCTACAA–3′
Fgf23	5′–ACTTGTCGCAGAAGCATC–3′	5′–GTGGGCGAACAGTGTAGAA–3′
Fgf2	5′–GTCACGGAAATACTCCAGTTGGT–3′	5′–CCCGTTTTTGGATCCGAGTTT–3′
Fgfr1	5′–GACTGCTGGAGTTAATACCA–3′	5′–CTGGTCTCTCTTCCAGGGCT–3′
Fgfr3	5′–GTTCTCTCTTTGTAGACTGC–3′	5′–AGTACCTGGCAGCACCA–3′
Ocn	5′–GAGGGCAATAAGGTAGTGAACAGA–3′	5′–AAGCCATACTGGTTTGATAGCTCG–3′
Op	5′–CCAGGTTTCTGATGAACAGTATCC–3′	5′–ACTTGACTCATGGCTGCCCTTT–3′
Opg	5′–CACCATCAGCTGAAGATAGT–3′	5′–CCAAGATCTCTAACATGACG–3′
Dmp1	5′–CAACTGGCTTTTCTGTGGCAA–3′	5′–TGGGTGCGCTGATGTTTGCT–3′
Mgp	5′–GTGGCGAGCTAAAGCCCAA–3′	5′–CGTAGCGCTCACACAGCTTG–3′
Sost	5′–CCTCCTCCTGAGAACAACCA–3′	5′–GCCGGAGCACACCAACTC–3′
Osterix	5′–ACTGGCTAGGTGGTGGTCAG–3′	5′–GGTAGGGAGCTGGGTTAAGG–3′
Runx2	5′–ACAAACAACCACAGAACCACAAAGT–3′	5′–GTCTCGGTGGCTGGTAGTGA–3′
Col1	5′–GGTCCTCGTGGTGCTGCT–3′	5′–ACCTTTGCCCCCTTCTTTG–3′
Lrp4	5′–TCTGCGCACACGGAATAG–3′	5′–GCGCTCACCGCACATGT–3′
Lrp5	5′–ACCCGCTGGACAAGTTCATC–3′	5′–TCTGGGCTCAGGCTTTGG–3′
Lrp6	5′–GGTGTCAAAGAAGCCTCTGC–3′	5′–ACCTCAATGCGATTTGTTCC–3′
Rankl	5′–CACCATCAGCTGAAGATAGT–3′	5′–CCAAGATCTCTAACATGACG–3′
Phex	5′–ATTAGGTGCCGAGAGGAAGA–3′	5′–TCCCCACAACATATGGGAGT–3′
Mepe	5′–ACTATCCACAAGTGGCCTCG–3′	5′–CCGCTGTGACATCCCTTTAT–3′
Dkk1	5′–ACTACCAGCCCTACCCTTGC–3′	5′–CTTGGACCAGAAGTGTCTTGC–3′
Sprty1	5′–TGTGTTCTTTGTGGCAGAGC–3′	5′–CGGCTATTCCAAGCTCACTC–3′
Sprty2	5′–ACATCGCTGGAAGAAGAGGA–3′	5′–CTGGGTAAGGGCATCTCTTG–3′
Sprty3	5′–GGGGGAGGGTGTGAGATAAT–3′	5′–TTGCCATGACAGCCATAAAA–3′
Sprty4	5′–TCTAGCTCTGGCGGAGCTGT–3′	5′–GTGAATCCCAGCTCAGTCAT–3′
Sef	5′–AACAGCCGACTGCACAACAT–3′	5′–GCAAGCGTACTGGCTGATG–3′
Wnt10b	5′–TTCTCTCGGGETTTCTTGGATTC–3′	5′–CCATGTGTCTCCCACGGACTGGCAG–3′
Npt2a	5′–CTGATTGTGGGTGCCCAACATGATG–3′	5′–TGCACTTCCGCTTCAGGTTTTC–5′

obtain a 7-μm longitudinal central section that includes the central vein. Sections were collected on a special cold adhesive tape Cryofilm type IIC (FINETEC Co. Ltd., Japan). Unstained tapes with samples were soaked in PBS for half an hour and then mounted in 50% glycerol in PBS for dynamic parameter analysis. Additional sections were stained for tartrate-resistant acid phosphatase to visualize osteoclasts and counterstained with hematoxylin. Histomorphometric measurements were made in a blinded, nonbiased manner using the OsteoMeasure image analysis system (R & M Biometrics, Nashville, TN) interfaced with a Nikon E400 microscope (Nikon Inc., Melville, NY). The terminology and units used are those recommended by the Histomorphometry Nomenclature Committee of the American Society for Bone and Mineral Research (31). Mineralizing surface/bone surface (MS/BS), the bone formation rate (BFR/BS), interlabel thickness, mineral apposition rate (MAR, μm/day), bone volume fraction (BV/TV), percent osteoblast surface, osteoclast surface, and osteoclast number/BS were measured. Osteoblasts were identified as cuboidal cells lining the trabecular bone. Osteoclasts were identified as multinucleated cells with more than three nuclei on the trabecular bone surface.

For cortical dynamic histomorphometry, longitudinal sections were used. Periosteal and endosteal parameters were measured along 1 mm, beginning 600 μm below the chondroosseous junction on both lateral and medial sides of the distal femur (32). Parameters measured include MS/BS, MAR, BFR/BS.

BMSCs Culture—BMSCs were extracted from excised tibial bones as described previously (11). BMSCs were plated in 6-well dishes at 2 million/well with 2 ml of minimum essential medium α (Invitrogen) + 10% FBS + penicillin/streptomycin. On day 3, the media were changed to minimum essential medium α + 10% FBS + 50 μM ascorbic acid + 4 mM β-glycerophosphate. The medium was changed every other day. These cells were cultured for 7, 14, or 21 days before takedown.

The fixed cultures were stained with alkaline phosphatase (ALP) according to the manufacturer's instructions. After plates were scanned, the plates were counter-stained for mineral by von Kossa stains. The HMWKO and WT wells were compared and analyzed using ImageJ (version 1.61, National Institutes of Health, Bethesda).

RNA Isolation and Real Time PCR—Total RNA was extracted from the flushed tibial bones using TRIzol reagent (Invitrogen). For real time quantitative RT-PCR analysis, RNA was reverse-transcribed by the Super-Script™ first-strand synthesis system. Quantitative PCR was carried out using the QuantiTect™ SYBR Green PCR kit (Qiagen) on a MyiQ™ instrument (Bio-Rad). β-Actin was used as an internal reference for each sample. mRNA was normalized to the β-actin mRNA level and expressed as the fold-change relative to the first sample for each experimental group. Relative mRNA expression was calculated using a formula reported previously (33). The primers for the genes of interest are listed in Table 1.

Western Blot Analysis—Protein was extracted from whole hearts using 1× RIPA buffer (Cell Signaling). Protein concentrations were measured with BCA protein assay reagent (Pierce). Tibial protein was purified utilizing protein A/G PLUS-agarose immunoprecipitation reagent, sc-2003 (Santa Cruz Biotechnology), according to the manufacturer's instructions. Protein was fractionated (tibia 250 μg and heart 300 μg) on SDS-polyacrylamide gel and transferred onto a PVDF membrane (Bio-Rad). Membrane was blocked for 1 h with 5% nonfat dry milk and then incubated overnight at 4 °C with anti-FGF2 (1:1000 Santa Cruz Biotechnology). Membranes were incubated with appropriate secondary antibody 1:20,000 (Amersham Bioscience) at room temperature for 1 h. Blots were developed with ECL plus reagents (Amersham Bioscience). Finally, blots were reprobed with actin antibody (Santa Cruz Biotechnology).
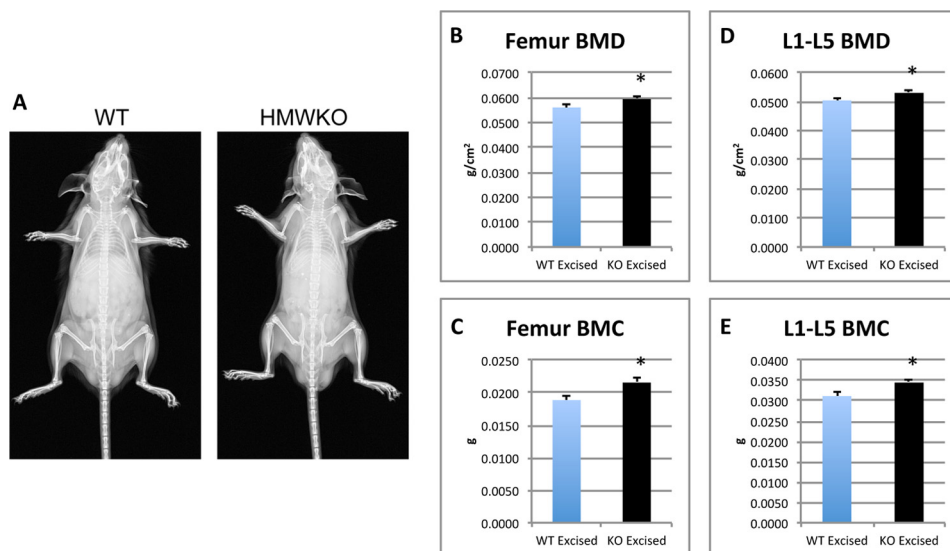
FIGURE 1. **X-ray images show no differences in HMWKO *versus* WT mice and dual beam x-ray absorptiometry analysis of excised femurs and vertebrae display increased BMD/BMC in HMWKO.** *A*, x-ray images of WT and HMWKO mice. Dual beam x-ray measurements are as follows: *B*, femur BMD; *C*, femur BMC; *D*, L1–5 BMD; *E*, L1–5 BMC. Values are the mean ± S.E. (*n* = 15–27) * indicates significantly different from WT group (*p* < 0.05).

Statistical Analyses—Experimental values were reported as means ± S.E. *t* test or analysis of variance followed by least significant difference for post hoc multiple comparisons were used. SPSS software was used for statistical analysis, and the results were considered significantly different at *p* < 0.05.

RESULTS

HMWFGF2KO Mouse Phenotype—Body weight was similar in HMWKO and WT littermates (data not shown). Radiographic examination (Fig. 1*A*) revealed no dwarfism or shortening of the limbs, in contrast to what was observed in the HMWTg mice (10).

Dual Beam X-ray Absorptiometry—To examine the effect of knock-out of the HMW isoforms on bone mass and the effect on different bone compartments, BMD and BMC were measured both *in vivo* and after bones were excised. *In vivo* whole body BMD was significantly increased by 11.3% (*p* < 0.05) and BMC by 23.2% (*p* < 0.05) in the HMWKO compared with WT (data not shown). *In vivo* BMD of the femurs was significantly increased by 9% (*p* < 0.05) and BMC by 18% (*p* < 0.05) (data not shown). *In vivo* BMD of the HMWKO L1 to L5 vertebrae was significantly increased by 10% (*p* < 0.05), and the BMC significantly increased by 15% (*p* < 0.05) compared with the WT (data not shown). BMD of excised femurs (Fig. 1*B*) was significantly increased by 5.9% (*p* < 0.05) and BMC (Fig. 1*C*) by 14.3% (*p* < 0.05) from the HMWKO. There was also a significant increase of BMD (Fig. 1*D*) and BMC (Fig. 1*E*) in excised L1 to L5 vertebrae of 5 and 10%, respectively (*p* < 0.05), in HMWKO when compared with WT littermates. The bone area of the femurs was slightly increased in the HMWKO but was not significantly different from the WT mice (data not shown). The excised measurements further support the increased bone mass phenotype observed in the HMWKO *in vivo*. These data suggest that KO of HMW increases bone mass in mice.

Micro-CT—Micro-CT was utilized to analyze the micro-architecture of the trabecular and cortical bone of the femurs of the HMWKO mice and WT littermates (Fig. 2*A*). In HMWKO,

trabecular bone volume (BV/TV) (Fig. 2*B*) was significantly increased by 75.8% (*p* < 0.05), trabecular thickness (Fig. 2*C*) by 17.65% (*p* < 0.05), and trabecular number (Fig. 2*D*) by 16.6% (*p* < 0.05) compared with WT. As shown in Fig. 2*E*, trabecular spacing was significantly reduced by 14.8% (*p* < 0.05) in HMWKO. Connective tissue density (Fig. 2*F*) was significantly increased by 103% (*p* < 0.05) in the HMWKO.

Micro-CT analysis of femur cortical bone (Fig. 3*A*) showed that the sub-periosteal area (Fig. 3*B*) was significantly increased by 25.1% (*p* < 0.05) in HMWKO. Cortical thickness (Fig. 3*C*) was also significantly increased by 20.4% (*p* < 0.05) in HMWKO. Cortical mask (Fig. 3*D*) was significantly increased by 32.7% (*p* < 0.05), and cortical porosity (Fig. 3*E*) was significantly reduced by 27.8% (*p* < 0.05). The volume of the bones was slightly increased in the HMWKO but was not significantly different from the WT (data not shown). The results from the micro-CT indicate that HMWKO have more structurally sound microarchitecture, and they also display increased bone mass in both the trabecular and cortical compartments.

Bone Histomorphometry—To determine whether increased bone mass in HMWKO was due to increased bone formation or decreased bone resorption, histomorphometric analysis was conducted on the femurs. Static histomorphometric analysis (Fig. 4*A*) revealed less tartrate-resistant acid phosphatase staining in the HMWKO *versus* the WT. Osteomeasure analysis (Fig. 4*B*) showed a significant increase of 80% BV/TV (*p* < 0.05) in the HMWKO. Osteoblast surface/bone surface (Fig. 4*C*) was significantly increased by 88% (*p* < 0.05) in the HMWKO. There was a significant reduction, 25% (*p* < 0.05), of osteoclast surface (Fig. 4*D*) and a 22% reduction (*p* < 0.05) in osteoclast number/BS (Fig. 4*E*) in HMWKO compared with WT.

Dynamic histomorphometry was performed on trabecular bone of undecalcified femurs. Representative images of labeling are shown (Fig. 5*A*). The inter-label thickness (Fig. 5*B*) was significantly increased by 38.3% (*p* < 0.05) in the HMWKO compared with the WT. MAR (Fig. 5*C*) was significantly
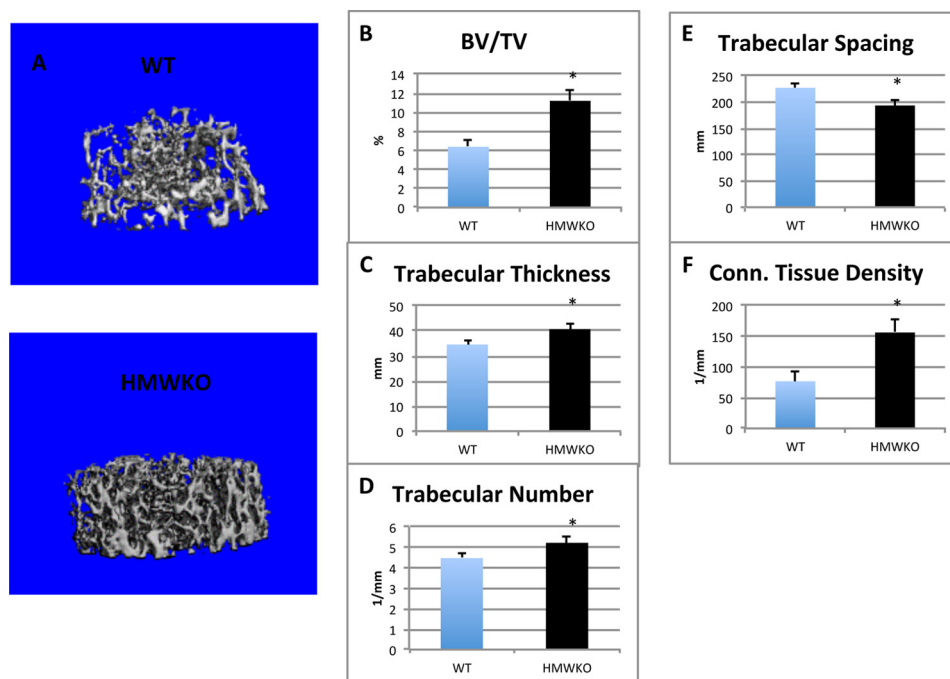
FIGURE 2. **Micro-CT analysis revealed increased trabecular bone measurements in HMWKO mice.** *A,* representative micro-CT three-dimensional trabecular structure of femurs of 2-month-old male mice. Three-dimensional trabecular microstructural parameters were calculated using two-dimensional data obtained from micro-CT, with calculated morphometric indices included. *B,* bone volume density; *C,* trabecular thickness; *D,* trabecular number; *E,* trabecular spacing; and *F,* connective (*Conn.*) tissue density. (*n* = 6) * indicates significantly different from WT group (*p* < 0.05).
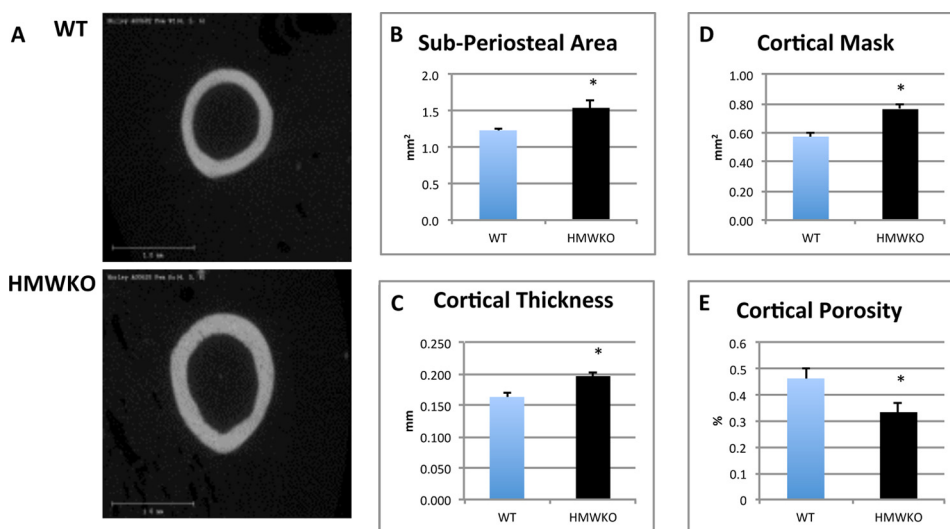

FIGURE 3. **HMWKO mice have increased cortical bone measurements when compared with WT mice by micro-CT.** *A,* representative micro-CT images of cortical bone. Cortical bone measurements are as follows: *B,* sub-periosteal area; *C,* cortical thickness; *D,* cortical mask; *E,* cortical porosity (*n* = 6). * indicates significantly different from WT (*p* < 0.05).

increased by 35.9% (*p* < 0.05) in HMWKO. The mineralizing surface per bone surface (MS/BS) (Fig. 5D) was significantly increased by 30.7% (*p* < 0.05) in HMWKO, and BFR/BS (Fig. 5E) was significantly increased by 89% in the HMWKO (*p* < 0.05). Taken together, these data show that knock-out of the HMW isoforms of FGF2 resulted in increased osteoblast activity and decreased osteoclast activity leading to a higher bone mass phenotype.

Dynamic histomorphometry of cortical bone is shown in Fig. 6. MAR, an index of osteoblast activity, in the periosteum was significantly increased by 79% in HMWKO mice (*p* < 0.05) compared with WT. MS/BS, an index of currently active min-

eralization, was significantly increased by 62% in HMWKO mice (*p* < 0.05) compared with WT. BFR/BS was significantly increased by 209% in HMWKO mice compared with WT (*p* < 0.05). There was no significant difference in MAR, MS/BS, and BFR/BS between WT and HMWKO in the cortical endosteum. Taken together, these data suggest that increased cortical bone is mediated by increased periosteal osteoblast function.

Alkaline Phosphatase-positive Colonies and Mineralized Nodules in Bone Marrow Cultures of WT and HMWKO Mice—We assessed whether HMWKO increased bone nodule formation *in vitro.* ALP-positive colonies were determined at days 7, 14, and 21 after initial culture. As shown in Fig. 7A, there was a
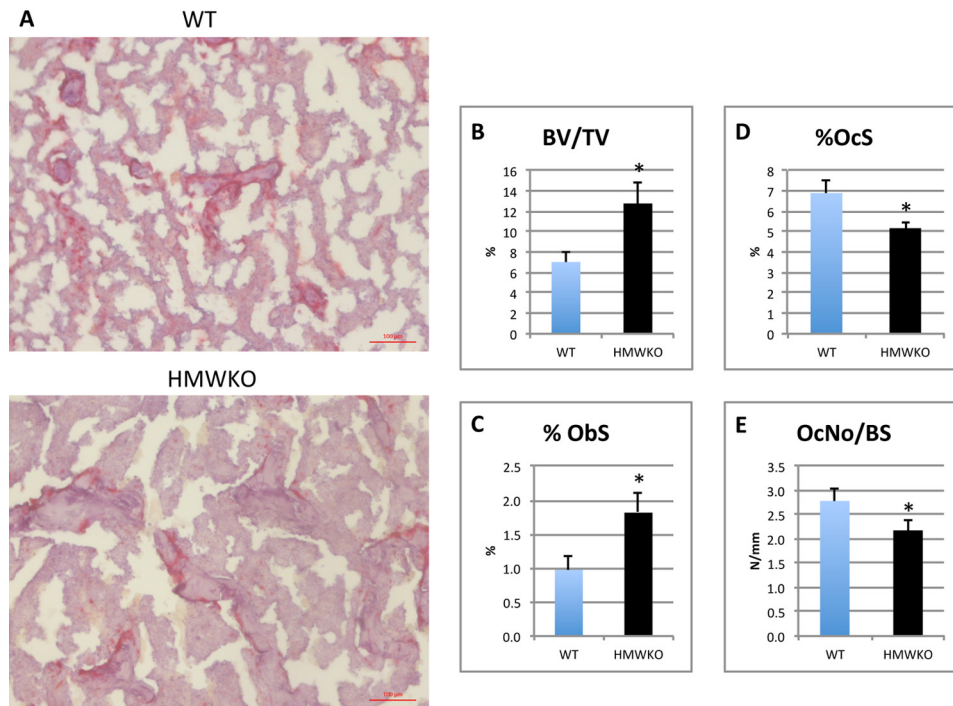
FIGURE 4. **Static bone histomorphometric analysis of trabecular bone in femurs showed HMWKO mice osteoblast/osteoclast activity favor bone mineralization.** *A,* ×10 representative images of tartrate-resistant acid phosphatase. *B,* BV/TV. *C,* percent osteoblast surface *(%ObS)*. *D,* percent osteoclast surface (*%OcS*); *E,* osteoclast number/bone surface (*OcNo/BS*) (n = 7–10). * indicates significantly different from WT ($p < 0.05$).
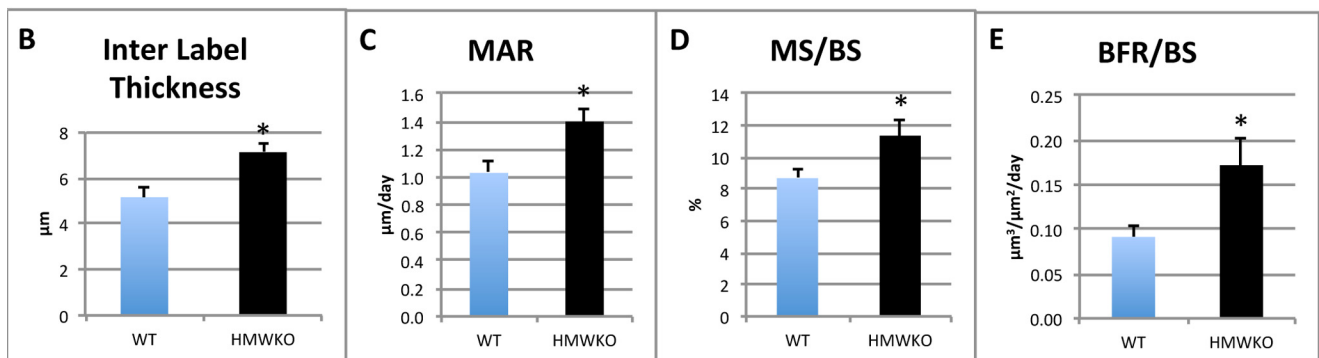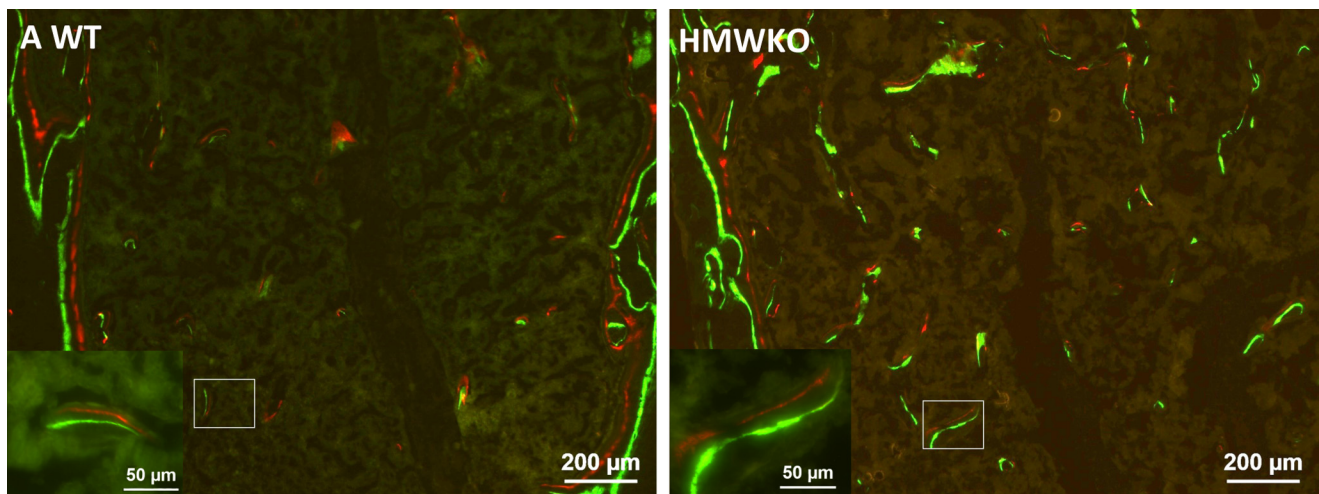

FIGURE 5. **Dynamic histomorphometric analysis of trabecular bone in femurs demonstrates increased bone mineralization rate in HMWKO mice.** *A,* fluorescent imaging of calcein and xylenol orange from representative WT and HMWKO mice utilizing a ×5 lens. Smaller image uses a ×20 lens. Dynamic histomorphometry measurements are as follows: *B,* inter-label thickness. *C,* mineral apposition rate (*MAR*). *D,* mineralizing surface/bone surface (*MS/BS*), and *E,* bone formation rate/bone surface (*BFR/BS*) (n = 9–10). * indicates significantly different from WT ($p < 0.05$).
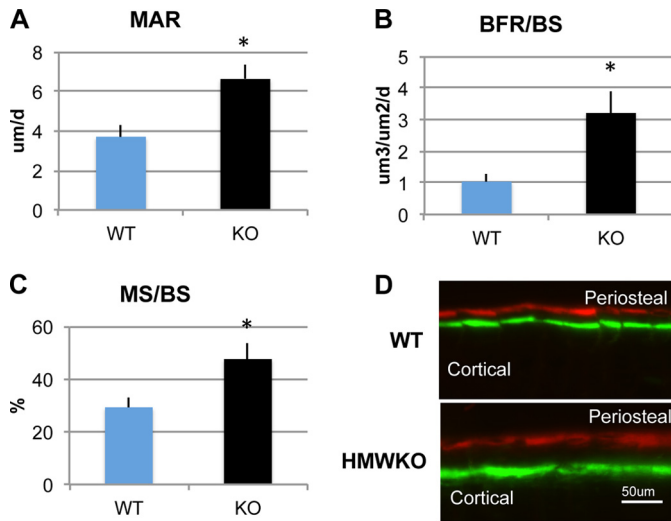
FIGURE 6. **Dynamic histomorphometric analysis of cortical bone of femurs from WT and HMWKO mice.** Dynamic histomorphometry measurements are as follows: *A,* mineral apposition rate (*MAR*); *B,* bone formation rate/bone surface (*BFR/BS*); and *C,* mineralizing surface/bone surface (*MS/BS*) in periosteal layer. * indicates significantly different from WT ($p < 0.05$). $n = 9$. *D,* fluorescent imaging of calcein and xylenol orange labeling in periosteum from representative WT and HMWKO mice.

greater increase in ALP-positive colonies in HMWKO cultures at 7, 14 and 21 days, and von Kossa staining showed that there was a greater increase in mineralized colonies at 21 days in HMWKO (Fig. 7*B*) compared with WT. At day 7, ALP+ colony number (Fig. 7*C*) was significantly increased by 52.6% in HMWKO ($p < 0.05$) when compared with the WT. The total ALP colony area was also calculated at 7, 14, and 21 days after initial culture (Fig. 7*D*) and was significantly increased ($p < 0.05$) in HMWKO at all time points. As shown in Fig. 7*E,* quantification of von Kossa-stained mineralized colony area was similar in HMWKO and WT on days 7 and 14; however, on day 21 the colony area was significantly increased by 94.9% ($p < 0.05$) compared with the WT. The increased ALP and von Kossa staining in HMWKO BMSC cultures is consistent with both enhanced proliferative and mineralization abilities, respectively.

Differential Bone Marker Gene Expression—To further investigate the bone phenotype observed in the HMWKO, mRNA expression levels of genes involved in osteoblast differentiation, matrix mineralization, and resorption were measured in the flushed tibias of HMWKO and WT mice (Fig. 8). In the HMWKO type 1 collagen (*Col1a1*) (Fig. 8*A*), mRNA was significantly increased by 131% ($p < 0.05$). Genes important in osteoblast differentiation such as Runt-related transcription factor 2 (*Runx2*) (Fig. 8*B*) were significantly increased by 39.6% ($p < 0.05$); osterix (Fig. 8*C*) was significantly increased by 48.1% ($p < 0.05$); and osteocalcin (*Oc*) (Fig. 8*D*) by 213% ($p < 0.05$) and osteopontin (*Op*) (Fig. 8*E*) by 118% ($p < 0.05$), compared with WT. Dentin matrix phosphoprotein-1 (*Dmp1*) (Fig. 8*F*) was significantly increased by 41.8% ($p < 0.05$) in HMWKO. Phosphate-regulating neutral endopeptidase, X-linked gene (*Phex*) (Fig. 8*G*), was increased by 48.2% in the HMWKO compared with WT, but this was not statistically significant. The expression of several matrix inhibitory genes was also measured. In contrast to our observation in bones of HMWTg mice, where

there was a marked increase in inhibitory *Mgp* (10), mRNA expression was similar in WT and HMWKO (Fig. 8*H*). Matrix extracellular phosphoglycoprotein (*Mepe*) mRNA (Fig. 8*J*) was similar in WT and HMWKO.

The effect of HMWKO on several components of the Wnt signaling pathway important in osteoblast differentiation was also examined. The receptors for *Sost*, low density lipoprotein receptor-related protein 4 (*Lrp4*), *Lrp5*, and *Lrp6* were not significantly different in the HMWKO compared with WT (data not shown). Dickkopf-related protein 1 (*Dkk1*), canonical Wnt signaling antagonist (34), was also measured, and there was a decrease in HMWKO, but it was not significantly different (Fig. 8*I*). *Wnt10b*, a Wnt ligand, also revealed no significant difference between the two groups (data not shown).

We also determined whether selective HMWKO modulated the mRNA levels for *Fgf2* and *Fgf23* (Fig. 9). *Fgf2* mRNA (Fig. 9*A*) was significantly reduced by 64.6% ($p < 0.05$). *Fgf23* (Fig. 9*B*) mRNA was significantly decreased by 35.4% ($p < 0.05$) in the HMWKO compared with WT. The mRNA levels of *Sprouty 1–4* genes and Sef, negative feedback regulators of *Fgf2* signaling through *FGFRs* (35), were not significantly different (data not shown). The quantitative PCR analysis of osteoclast-related genes, receptor activator of *Nfkb* (*Rankl*), and osteoprotegerin (*Opg*) revealed a decrease in the receptor activator of NF-κB ligand/OPG ratio in the HMWKO, which was not significant (data not shown).

We also examined the effect of HMWKO on the sodium-phosphate transporter gene *Npt2a* in the kidneys. The mRNA levels of *Npt2a* in the kidneys of HMWKO mice were not significantly different from WT mice (data not shown).

Biochemistry—Serum levels of FGF23, PTH, calcium, and phosphate were determined as described under "Experimental Procedures." Serum FGF23 level in HMWKO mice was not significantly different from WT (Fig. 10*A*). Serum calcium was also similar in WT and HMWKO (Fig. 10*B*). Interestingly in contrast to HMWTg mice in which serum PTH was significantly increased and serum P$_i$ was significantly decreased (10), we observed levels of serum PTH (Fig. 10*C*) and serum P$_i$ (Fig. 10*D*) in HMWKO that were similar to WT.

We examined SOST/sclerostin expression in serum and bones of WT and HMWKO mice. Serum sclerostin was significantly decreased in the HMWKO compared with the WT (Fig. 11*A*). As shown in Fig. 11*B*, there was a significant reduction of 65% ($p < 0.05$) in *Sost* mRNA in bones from HMWKO. Immunofluorescent representative images of sclerostin protein in femurs from WT and HMWKO (Fig. 11*C*) are shown. Reduced sclerostin immunofluorescence labeling is seen in osteocytes of HMWKO.

Western Blot Analysis—To confirm that HMW protein isoforms were not expressed in the HMWKO mouse model, Western blots of heart and tibia protein were utilized to confirm the absence of the HMW FGF2 protein isoforms (data not shown). Both HMW and LMW isoforms were expressed in WT. However in the HMWKO only the LMW isoform was expressed.

DISCUSSION

This study demonstrates that mice with selective deletion of nuclear HMW FGF2 isoforms have a phenotype characterized
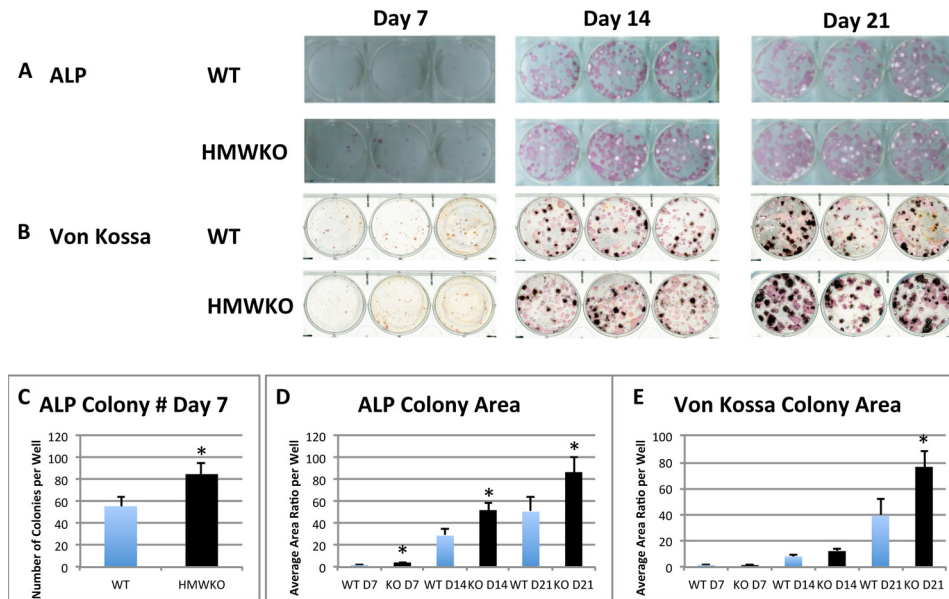
FIGURE 7. **Increased alkaline phosphatase-positive colonies and mineralized nodules in bone marrow cultures from HMWKO mice *versus* WT cultures.** *A,* representative images of ALP-positive colonies at days 7, 14, and 21 of culture. *B,* representative images of von Kossa staining at days 7, 14, and 21 of culture. *C,* quantitative analysis of ALP-positive colony number; *D,* ALP-positive colony area measured by ImageJ software (National Institutes of Health). Number of wells measured at day 7 ($n = 15$ for WT and KO), day 14 (WT, $n = 15$; KO, $n = 21$), and day 21 (WT, $n = 17$; KO, $n = 21$). *E,* quantitative analysis of von Kossa-positive colony area utilizing ImageJ software. Number of wells measured at day 7 ($n = 15$ for WT and KO), day 14 (WT, $n = 14$; KO, $n = 20$), and day 21 (WT, $n = 16$; KO, $n = 21$). * indicates significantly different from WT ($p < 0.05$).
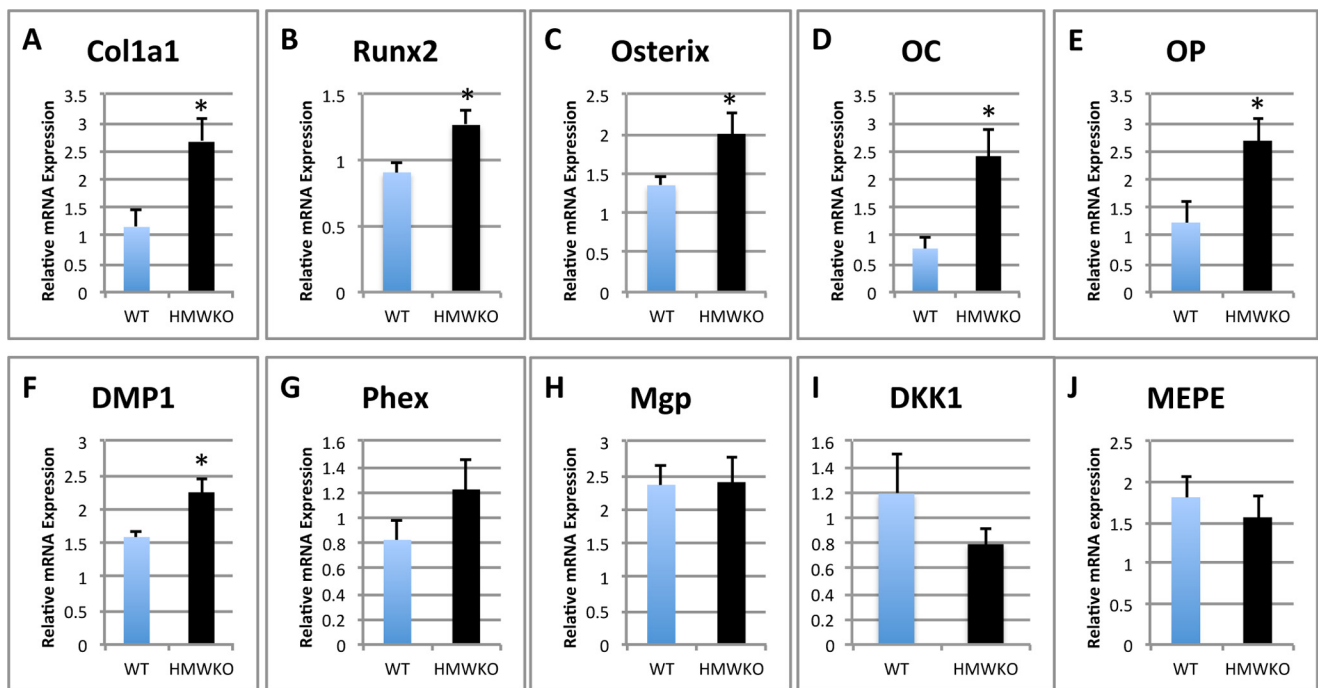

FIGURE 8. **Transcriptional regulation in HMWKO mice favors expression of genes that promote osteoblast differentiation and matrix mineralization in bone.** Shown is real time RT-PCR analysis of *Col1a1* (A), *Runx2* (B), osterix (C), *OC* (D), *Op* (E), *Dmp1* (F), *Phex* (G), *Mgp* (H), *Dkk1* (I), and *Mepe* (J) mRNA expression in flushed tibial bones ($n = 7–13$). * indicates significantly different from WT ($p < 0.05$).

by lack of dwarfism, increased BMD and BMC, as well as normal serum P_i and PTH. The increase in BMD and BMC, increased structural and functional parameters of bone as determined by micro-CT, and static and dynamic histomorphometry indicate increased bone mass and promotion of bone mineralization in the absence of the HMW isoforms of FGF2. *In vitro* osteogenic cultures also support the conclusion that knock-out of the HMWFGF2 isoforms results in increased dif-

ferentiation and mineralization phenotype. Taken together, the data support the conclusion that HMWFGF2 isoforms negatively regulate osteoblast activity and bone mineralization.

Micro-CT and BMD demonstrated increased bone thickness and density in HMWKO. They have improved structural integrity demonstrated by significantly increased trabecular number, increased trabecular thickness, and significantly decreased trabecular spacing. Cortical thickness was also improved,
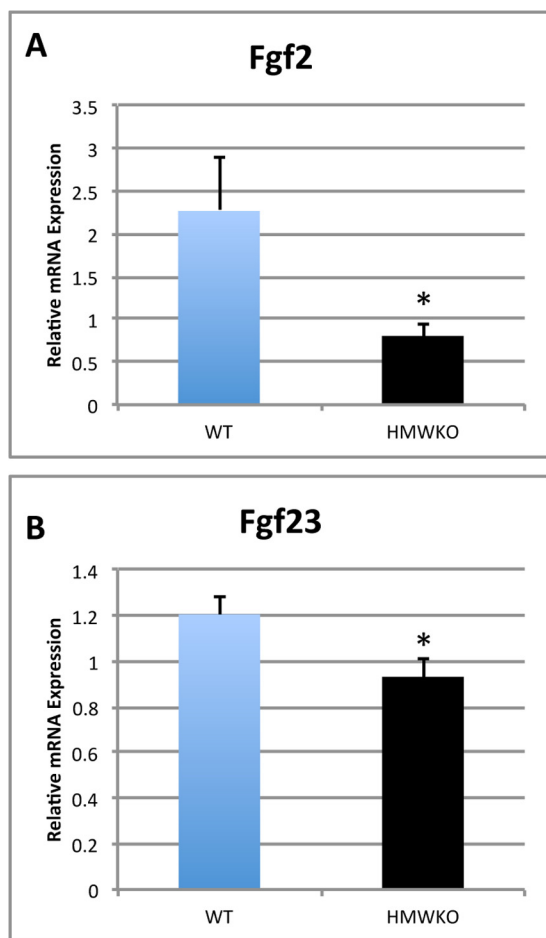
FIGURE 9. Modulation of *Fgf2* and *Fgf23* mRNA in HMWKO bones. Shown is real time RT-PCR analysis of *Fgf2* (*A*) and *Fgf23* (*B*) mRNA expression in flushed tibial bones ($n = 7–11$). * indicates significantly different from WT ($p < 0.05$).

which contributes to bone strength (36). These data indicate improvement of bone integrity and formation in both the trabecular and cortical compartments. All of these structural measurements indicate that HMWKO mice have improved bone structural integrity and might have decreased potential for fractures.

It is known that HMWFGF2 modulates bone formation and P_i homeostasis by causing increases in *Fgf23* mRNA and protein levels in HMWTg mice (10). HMWFGF2 can function as intracrine signals through FGF receptors that translocate into the nucleus via importin-β-mediated transport (37). When bound to FGF2 ligands, the complexes can function as transcriptional activators (37) to regulate Fgf23 (11). FGF23 produced by osteoblasts/osteocytes is released into the circulation to affect P_i homeostasis via the kidney. In the absence of HMWFGF2 isoforms, the increased bone mass and structural integrity could partially be accounted for by the decrease in *Fgf23* expression in bone and improved phosphate reabsorption by Npt2a in the kidney, leading to normal serum levels of phosphate. However, this alone may not be responsible for the increased bone mass phenotype in the HMWKO because modulation of osteoblast-related genes could contribute to the increased bone mass phenotype. Specifically, in contrast to the HMWTg mice (10, 11) in which a number of osteoblast differentiation promoting

genes such as *Runx2*, osterix, and *OC* and pro-mineralization genes such as *Phex* and *Dmp1* were decreased and inhibitory genes such as Mgp and Sost were increased, we observed increased expression of *Runx2*, osterix, *OC*, and *Dmp*1, normal expression of Mgp, and markedly reduced expression of *Sost* in the bones of HMWKO mice. The level of *Col1a1* mRNA expression was significantly increased in the HMWKO mouse model, but it was significantly decreased in the HMWTg mice previously studied (10). The reduced expression of Col1a1 in the HMWTg could limit the available scaffolding area for bone formation, contributing to the observed reduced bone mass phenotype.

Expression levels of *Mgp*, a calcification inhibitor (28), were identical when HMWKO and WT were compared in this study. However, in our previous study, *Mgp* mRNA was increased by 446% in tibial bones of HMWTg mice when compared with the vector (10). These data indicate that the nuclear isoforms of FGF2 may directly affect the promotion of the expression of the calcification inhibitor *Mgp*. The HMW isoform of FGF2 may only mediate this effect of *Mgp* when its own expression is increased beyond the baseline. The ability of the cell to rapidly increase *Mgp* expression could be vital when attempting to slow bone mineralization during normal bone development or under conditions such as fracture repair.

In addition to *Mgp*, sclerostin, the product of the *Sost* gene also inhibits osteoblast differentiation and bone formation via binding of *Lrp4/5/6*, which blocks canonical Wnt signaling in osteoblasts (38–40). *Sost* mRNA expression was significantly decreased in HMWKO mice and increased in the HMWTg (10). Sclerostin was also significantly decreased in the serum of HMWKO mice. Sclerostin also functions to inhibit bone formation through modulation of the Phex/Mepe ASARM pathway (38) by increasing Mepe-ASARM protein that competitively binds with Phex inhibiting activation of Dmp1 (26). Activated Dmp1 is able to nucleate hydroxyapatite crystals during the initiation of bone formation (39). Thus, modulation of *Sost* could be a main pathway by which HMWFGF2 modulates bone homeostasis.

Enhanced Wnt signaling in HMWKO due to reduced *Sost* could over a period of time possibly promote tumor development, but this has not been observed in the HMWKO mice that have been aged.

In addition to its effects on osteoblast differentiation and matrix mineralization, HMW also appear to affect osteoclast number and function, because we observed reduced OCL parameters by histomorphometry in HMWKO. We also observed normal serum PTH. This result is of interest because PTH increases osteoclastic bone resorption and P_i wasting. Normal serum PTH and reduced osteoclast number and activity in HMWKO mice are in contrast to our observations in the HMWTg where we reported significantly increased OCL number and OCL surface by histomorphometry as well increased serum PTH and serum carboxyl-terminal collagen cross-links, a marker of increased bone turnover (10). Thus, decreased osteoclast activity could contribute to the increased bone mass phenotype in HMWKO mice. The role of PTH in the normalization of serum P_i in HMWKO is further intriguing because we previously reported that PTH increased HMWFGF2 nuclear accumulation in osteoblastic MC3T3-E1 cells and transcriptionally
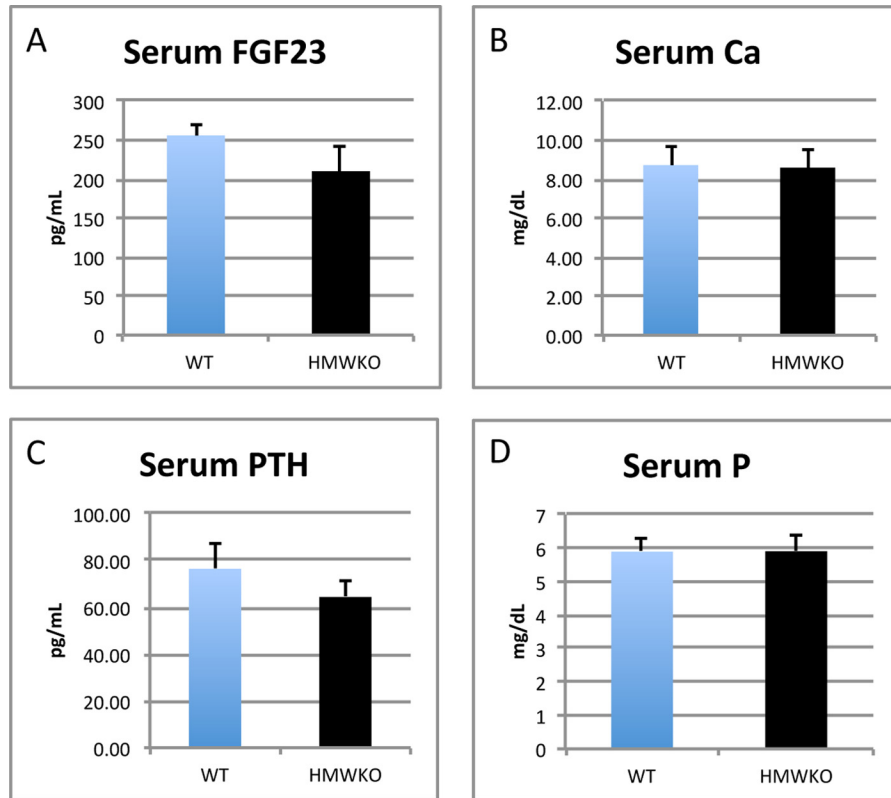
FIGURE 10. **Serum FGF23, calcium, PTH, and phosphate levels were not significantly different in WT and HMWKO.** *A,* serum FGF23. *B,* serum calcium. *C,* serum PTH. *D,* serum phosphate. Serum FGF23 and PTH ($n = 8$–10). Serum calcium and P_i ($n = 16$–19).
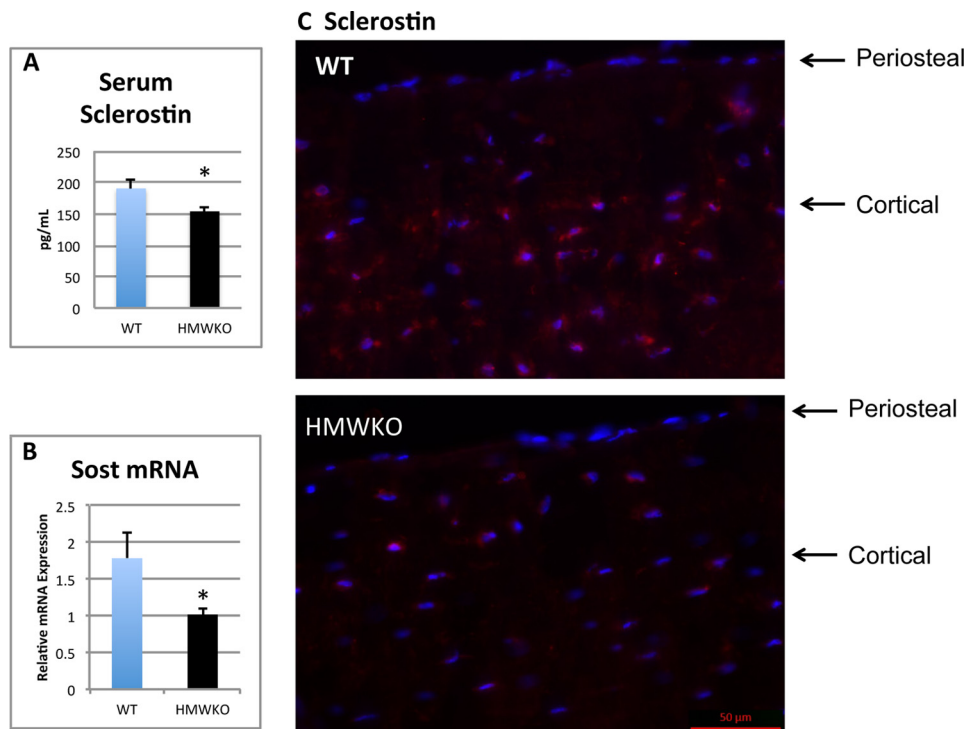

FIGURE 11. **Decreased serum sclerostin and decreased *Sost* mRNA and protein in bones of HMWKO mice compared with WT.** *A,* serum sclerostin. *B,* RT-PCR *Sost* mRNA. *C,* representative immunofluorescent images for sclerostin expression in femurs. Decreased sclerostin expression (*red*) in osteocytes of cortical bone in HMWKO compared with WT. Nuclei were counterstained with DAPI (*blue*) (serum $n = 10$–11). * indicates significantly different from WT ($p < 0.05$).

regulated *Fgf2* promoter luciferase activity (42). These novel findings, when combined with the previously published data (10, 11), suggest that the HMW isoforms of FGF2 have inhibi-tory action on bone formation that are in addition to their ability to suppress mineralization by increasing Fgf23 expression and enhancing phosphate wasting.

In addition to the novel data that mice without the nuclear isoforms of FGF2 have increased bone mineral density and structural integrity, our previous studies investigated the overexpression of either the HMW or LMW isoforms of FGF2. When the results of all of these studies are taken into account, the data suggest that HMW nuclear isoforms of FGF2 may have some dominant function over the LMW isoform, the latter of which promotes bone formation, in a wild-type mouse when both are expressed. In mice that have all isoforms of FGF2 knocked out, there is a decrease in BMD and BMC (43). When only the LMW isoform is transgenically overexpressed, there is a dramatic increase in BMD and BMC (8). When the LMW isoform is knocked out, the mice present with significantly lower BMD and BMC than their WT littermates (8). HMWTg mice display a phenotype of decreased BMD and BMC (10). When all FGF2 isoforms are globally overexpressed, the mice display defective bone mineralization and osteopenia (6, 7). To account for these differential effects, the HMW isoforms could modulate the expression of the LMW isoform by promoting transcription of the HMWFGF2 from the unconventional CUG start codons upstream from the conventional start codon of the LMW isoform. Another possible mechanism for the dominant function of the HMW isoforms could be through competitive binding of the nuclear FGFR1 affecting the signaling ability of the LMW isoform (44). HMWFGF2 could also function as a negative feedback loop to halt bone formation after fracture repair by stimulating osteoclast bone resorption and Mgp calcification inhibition.

In summary, HMWFGF2 isoforms modulate bone and phosphate homeostasis via multiple pathways related to bone formation, osteoblast differentiation, and Wnt and Fgf2 signaling. The major players in this mechanism may be *Sost* and *Fgf23*, which is also linked to left ventricular hypertrophy (41, 45). The relationship of the isoforms of FGF2 to bone and phosphate homeostasis is beginning to be understood. Once the complete mechanisms of function are determined, proper manipulation of the Fgf2 pathways may prove to be beneficial in a clinical setting.

REFERENCES

1. Gospodarowicz, D. (1990) Fibroblast growth factor. Chemical structure and biologic function. *Clin. Orthop. Relat. Res.* **257,** 231–248
2. Arnaud, E., Touriol, C., Boutonnet, C., Gensac, M. C., Vagner, S., Prats, H., and Prats, A. C. (1999) A new 34-kilodalton isoform of human fibroblast growth factor 2 is cap dependently synthesized by using a non-AUG start codon and behaves as a survival factor. *Mol. Cell. Biol.* **19,** 505–514
3. Okada-Ban, M., Thiery, J. P., and Jouanneau, J. (2000) Fibroblast growth factor-2. *Int. J. Biochem. Cell. Biol.* **32,** 263–267
4. Prats, H., Kaghad, M., Prats, A. C., Klagsbrun, M., Lélias, J. M., Liauzun, P., Chalon, P., Tauber, J. P., Amalric, F., and Smith, J. A. (1989) High molecular mass forms of basic fibroblast growth factor are initiated by alternative CUG codons. *Proc. Natl. Acad. Sci. U.S.A.* **86,** 1836–1840
5. Sørensen, V., Nilsen, T., and Wiedłocha, A. (2006) Functional diversity of FGF-2 isoforms by intracellular sorting. *BioEssays* **28,** 504–514
6. Coffin, J. D., Florkiewicz, R. Z., Neumann, J., Mort-Hopkins, T., Dorn, G. W., 2nd, Lightfoot, P., German, R., Howles, P. N., Kier, A., and O'Toole, B. A. (1995) Abnormal bone growth and selective translational regulation in basic fibroblast growth factor (FGF-2) transgenic mice. *Mol. Biol. Cell* **6,** 1861–1873
7. Sobue, T., Naganawa, T., Xiao, L., Okada, Y., Tanaka, Y., Ito, M., Okimoto, N., Nakamura, T., Coffin, J. D., and Hurley, M. M. (2005) Overexpression of fibroblast growth factor-2 causes defective bone mineralization and osteopenia in transgenic mice. *J. Cell. Biochem.* **95,** 83–94
8. Xiao, L., Liu, P., Li, X., Doetschman, T., Coffin, J. D., Drissi, H., and Hurley, M. M. (2009) Exported 18-kDa isoform of fibroblast growth factor-2 is a critical determinant of bone mass in mice. *J. Biol. Chem.* **284,** 3170–3182
9. Delrieu, I. (2000) The high molecular weight isoforms of basic fibroblast growth factor (FGF-2): an insight into an intracrine mechanism. *FEBS Lett.* **468,** 6–10
10. Xiao, L., Naganawa, T., Lorenzo, J., Carpenter, T. O., Coffin, J. D., and Hurley, M. M. (2010) Nuclear isoforms of fibroblast growth factor 2 are novel inducers of hypophosphatemia via modulation of FGF23 and KLOTHO. *J. Biol. Chem.* **285,** 2834–2846
11. Xiao, L., Esliger, A., and Hurley, M. M. (2013) Nuclear fibroblast growth factor 2 (FGF2) isoforms inhibit bone marrow stromal cell mineralization through FGF23/FGFR/MAPK *in vitro*. *J. Bone Miner. Res.* **28,** 35–45
12. Lu, Y., and Feng, J. Q. (2011) FGF23 in skeletal modeling and remodeling. *Curr. Osteoporos. Rep.* **9,** 103–108
13. Yu, X., and White, K. E. (2005) Review FGF23 and disorders of phosphate homeostasis. *Cytokine Growth Factor Rev.* **16,** 221–232
14. Quarles, L. D. (2012) Skeletal secretion of FGF-23 regulates phosphate and vitamin D metabolism. *Nat. Rev. Endocrinol.* **8,** 276–286
15. Kurosu, H., Ogawa, Y., Miyoshi, M., Yamamoto, M., Nandi, A., Rosenblatt, K. P., Baum, M. G., Schiavi, S., Hu, M. C., Moe, O. W., and Kuro-o, M. (2006) Regulation of fibroblast growth factor-23 signaling by klotho. *J. Biol. Chem.* **281,** 6120–6123
16. Urakawa, I., Yamazaki, Y., Shimada, T., Iijima, K., Hasegawa, H., Okawa, K., Fujita, T., Fukumoto, S., and Yamashita, T. (2006) Klotho converts canonical FGF receptor into a specific receptor for FGF23. *Nature* **444,** 770–774
17. Kuro-o, M., Matsumura, Y., Aizawa, H., Kawaguchi, H., Suga, T., Utsugi, T., Ohyama, Y., Kurabayashi, M., Kaname, T., Kume, E., Iwasaki, H., Iida, A., Shiraki-Iida, T., Nishikawa, S., Nagai, R., and Nabeshima, Y. I. (1997) Mutation of the mouse klotho gene leads to a syndrome resembling aging. *Nature* **390,** 45–51
18. Jüppner, H. (2011) Phosphate and FGF-23. *Kidney Int. Suppl.* **79**(S121), S24–S27
19. Masuda, M., Yamamoto, H., Kozai, M., Tanaka, S., Ishiguro, M., Takei, Y., Nakahashi, O., Ikeda, S., Uebanso, T., Taketani, Y., Segawa, H., Miyamoto, K., and Takeda, E. (2010) Regulation of renal sodium-dependent phosphate co-transporter genes (Npt2a and Npt2c) by all-*trans*-retinoic acid and its receptors. *Biochem. J.* **429,** 583–592
20. Sapir-Koren, R., and Livshits, G. (2011) Bone mineralization and regulation of phosphate homeostasis. *IBMS BoneKey* **8,** 286–300
21. Wang, H., Yoshiko, Y., Yamamoto, R., Minamizaki, T., Kozai, K., Tanne, K., Aubin, J. E., and Maeda, N. (2008) Overexpression of fibroblast growth factor 23 suppresses osteoblast differentiation and matrix mineralization *in vitro*. *J. Bone Miner. Res.* **23,** 939–948
22. Touriol, C., Bornes, S., Bonnal, S., Audigier, S., Prats, H., Prats, A. C., and Vagner, S. (2003) Generation of protein isoform diversity by alternative initiation of translation at non-AUG codons. *Biol. Cell* **95,** 169–178
23. Beck, L., Soumounou, Y., Martel, J., Krishnamurthy, G., Gauthier, C., Goodyer, C. G., and Tenenhouse, H. S. (1997) Pex/PEX tissue distribution and evidence for a deletion in the 3′ region of the Pex gene in X-linked hypophosphatemic mice. *J. Clin. Invest.* **99,** 1200–1209
24. Lorenz-Depiereux, B., Bastepe, M., Benet-Pagès, A., Amyere, M., Wagenstaller, J., Müller-Barth, U., Badenhoop, K., Kaiser, S. M., Rittmaster, R. S., Shlossberg, A. H., Olivares, J. L., Loris, C., Ramos, F. J., Glorieux, F., Vikkula, M., Jüppner, H., and Strom, T. M. (2006) DMP1 mutations in autosomal recessive hypophosphatemia implicate a bone matrix protein in the regulation of phosphate homeostasis. *Nat. Genet.* **38,** 1248–1250
25. Larsson, T., Marsell, R., Schipani, E., Ohlsson, C., Ljunggren, O., Tenenhouse, H. S., Jüppner, H., and Jonsson, K. B. (2004) Transgenic mice expressing fibroblast growth factor 23 under the control of the α1(I) collagen

promoter exhibit growth retardation, osteomalacia, and disturbed phosphate homeostasis. *Endocrinology* **145,** 3087–3094

26. Rowe, P. (2012) Regulation of bone–renal mineral and energy metabolism: The PHEX, FGF23, DMP1, MEPE ASARM pathway. *Crit. Rev. Eukaryot. Gene Expr.* **22,** 61–86

27. Martin, A., Liu, S., David, V., Li, H., Karydis, A., Feng, J. Q., and Quarles, L. D. (2011) Bone proteins PHEX and DMP1 regulate fibroblastic growth factor Fgf23 expression in osteocytes through a common pathway involving FGF receptor (FGFR) signaling. *FASEB J.* **25,** 2551–2562

28. Zebboudj, A. F., Imura, M., and Boström, K. (2002) Matrix GLA protein, a regulatory protein for bone morphogenetic protein-2. *J. Biol. Chem.* **277,** 4388–4394

29. Azhar, M., Yin, M., Zhou, M., Li, H., Mustafa, M., Nusayr, E., Keenan, J. B., Chen, H., Pawlosky, S., Gard, C., Grisham, C., Sanford, L. P., and Doetschman, T. (2009) Gene targeted ablation of high molecular weight fibroblast growth factor-2. *Dev. Dyn.* **238,** 351–357

30. Montero, A., Okada, Y., Tomita, M., Ito, M., Tsurukami, H., Nakamura, T., Doetschman, T., Coffin, J. D., and Hurley, M. M. (2000) Disruption of the fibroblast growth factor-2 gene results in decreased bone mass and bone formation. *J. Clin. Invest.* **105,** 1085–1093

31. Parfitt, A. M., Drezner, M. K., Glorieux, F. H., Kanis, J. A., Malluche, H., Meunier, P. J., Ott, S. M., and Recker, R. R. (1987) Bone histomorphometry: standardization of nomenclature, symbols, and units. Report of the ASBMR Histomorphometry Nomenclature Committee. *J. Bone Miner. Res.* **2,** 595–610

32. Sims, N. A., Clément-Lacroix, P., Da Ponte, F., Bouali, Y., Binart, N., Moriggl, R., Goffin, V., Coschigano, K., Gaillard-Kelly, M., Kopchick, J., Baron, R., and Kelly, P. A. (2000) Bone homeostasis in growth hormone receptor–null mice is restored by IGF-I but independent of Stat5. *J. Clin. Invest.* **106,** 1095–1103

33. Pfaffl, M. (2001) A new mathematical model for relative quantification in real-time RT-PCR. *Nucleic Acids Res.* **29,** e45

34. Butler, J. S., Murray, D. W., Hurson, C. J., O'Brien, J., Doran, P. P., and O'Byrne, J. M. (2011) The role of Dkk1 in bone mass regulation: correlating serum Dkk1 expression with bone mineral density. *J. Orthop. Res.* **29,** 414–418

35. Edwin, F., Anderson, K., Ying, C., and Patel, T. B. (2009) Intermolecular interactions of sprouty proteins and their implications in development and disease. *Mol. Pharmacol.* **76,** 679–691

36. Ammann, P., and Rizzoli, R. (2003) Bone strength and its determinants. *Osteopor. Int.* **14,** S13–S18

37. Stachowiak, M. K., Fang, X., Myers, J. M., Dunham, S. M., Berezney, R., Maher, P. A., and Stachowiak, E. K. (2003) Integrative nuclear FGFR1 signaling (INFS) as a part of a universal "feed-forward-and-gate" signaling module that controls cell growth and differentiation. *J. Cell. Biochem.* **90,** 662–691

38. Atkins, G. J., Rowe, P. S., Lim, H. P., Welldon, K. J., Ormsby, R., Wijenayaka, A. R., Zelenchuk, L., Evdokiou, A., and Findlay, D. M. (2011) Sclerostin is locally acting regulator of late-osteoblast/preosteocyte differentiation and regulates mineralization through a MEPE-ASARM-dependent mechanism. *J. Bone Miner. Res.* **26,** 1425–1436

39. He, G., Dahl, T., Veis, A., and George, A. (2003) Nucleation of apatite crystals *in vitro* by self-assembled dentin matrix protein 1. *Nat. Mater.* **2,** 552–558

40. Kumar, J., Swanberg, M., McGuigan, F., Callreus, M., Gerdhem, P., and Akesson, K. (2011) LRP4 association to bone properties and fracture and interaction with genes in the Wnt- and BMP signaling pathways. *Bone* **49,** 343–348

41. Faul, C., Amaral, A. P., Oskouei, B., Hu, M. C., Sloan, A., Isakova, T., Gutiérrez, O. M., Aguillon-Prada, R., Lincoln, J., Hare, J. M., Mundel, P., Morales, A., Scialla, J., Fischer, M., Soliman, E. Z., Chen, J., Go, A. S., Rosas, S. E., Nessel, L., Townsend, R. R., Feldman, H. I., St John Sutton, M., Ojo, A., Gadegbeku, C., Di Marco, G. S., Reuter, S., Kentrup, D., Tiemann, K., Brand, M., Hill, J. A., Moe, O. W., Kuro-O, M., Kusek, J. W., Keane, M. G., and Wolf, M. (2011) FGF23 induces left ventricular hypertrophy. *J. Clin. Invest.* **121,** 4393–4408

42. Hurley, M. M., Tetradis, S., Huang, Y. F., Hock, J., Kream, B. E., Raisz, L. G., and Sabbieti, M. G. (1999) Parathyroid hormone regulates the expression of fibroblast growth factor-2 mRNA and fibroblast growth factor receptor mRNA in osteoblastic cells. *J. Bone Miner. Res.* **14,** 776–783

43. Xiao, L., Sobue, T., Esliger, A., Kronenberg, M. S., Coffin, J. D., Doetschman, T., and Hurley, M. M. (2010) Disruption of the Fgf2 gene activates the adipogenic and suppresses the osteogenic program in mesenchymal marrow stromal stem cells. *Bone* **47,** 360–370

44. Liao, S., Bodmer, J. R., Azhar, M., Newman, G., Coffin, J. D., Doetschman, T., and Schultz Jel, J. (2010) The influence of FGF2 high molecular weight (HMW) isoforms in the development of cardiac ischemia–reperfusion injury. *J. Mol. Cell. Cardiol.* **48,** 1245–1254

45. Kardami, E., Jiang, Z. S., Jimenez, S. K., Hirst, C. J., Sheikh, F., Zahradka, P., and Cattini, P. A. (2004) Fibroblast growth factor 2 isoforms and cardiac hypertrophy. *Cardiovasc. Res.* **63,** 458–466